Short Range Stiffness During Voluntary Contraction

Ilse van der Greft

April 2011

Student number: 1333925

Exam number: 1190

Graduation commission:

Prof. Dr. F.C.T. van der Helm, BMechE, 3ME

Dr. Ir. E. de Vlugt, BMechE, 3ME

Dr. J.H. de Groot, LUMC

Ir. G.J. van der Veen, DCSC, 3ME

TU Delft Delft University of Technology

LUMC LEIDEN UNIVERSITY MEDICAL CENTER

Content

Short Range Stiffness is equal in eccentric and concentric wrist joint loading

Paper

Ilse van der Greft

Delft University of Technology

Leiden University Medical Center

Short Range Stiffness is equal in eccentric and concentric wrist joint loading

Ilse van der Greft[1], Jurriaan H. de Groot[2], Stijn van Eesbeek[1], Frans C. T. van der Helm[1], Erwin de Vlugt[1]

[1] Department of Biomechanical Engineering, Faculty of Mechanical Engineering, Laboratory for Neuromuscular Control, Delft University of Technology, Mekelweg 2, 2628 CD Delft, The Netherlands
[2] Department of Rehabilitation Medicine, Leiden University Medical Center, Laboratory for Kinematics and Neuromechanics, Albinusdreef2, 2333 ZA Leiden, The Netherlands

Abstract

A bi-phasic force response is found in muscle stretch. Force response is high at the start of the stretch and drops at certain length. The high initial force response is referred to as Short Range Stiffness and the moment at which the force response drops is referred to as the elastic limit. It is likely that this bi-phasic torque response is caused by the properties of the contractile elements of the muscle. The first part of the force response is attributed to the elastic stretch of attached cross-bridges and the stiffness reduction is attributed to the breakage of cross bridges.

The aim of this study was to estimate Short-range stiffness in eccentric and concentric joint loading. Flexion and extension rotations were imposed to the wrist at 3 different velocities and at 4 voluntary contraction levels using a servo controlled electrical motor. A nonlinear model-based identification procedure was used to identify Short-range stiffness and the elastic limit from in vivo recordings of the human wrist joint. The results showed that Short-range stiffness was equal in concentric and eccentric loading. The decrease in stiffness after Short-range stiffness is greater in concentric loading compared to eccentric loading. The results corresponded well to the muscle force velocity relation.

1 Introduction

In a short range of muscle stretch, muscle force increases proportional with muscle length (Cui et al., 2007; Joyce et al., 1969; Petit et al., 1990; Rack and Westbury, 1974; Walmsley and Proske, 1981). When the elongation of the muscle continues, increase in muscle force drops at a certain length, referred to as the elastic limit (EL). The high initial force response is caused by stiffness from attached cross-bridges, which is referred to as short range stiffness (SRS). The reduction of stiffness beyond EL is attributed to forcible breakage of cross-bridges (Campbell and Lakie, 1998).

In joint rotation muscles are shortened while consequently other muscles are lengthened. Until now joint SRS has been quantified in eccentric loading where muscles lengthen. No attempts have been made so far to quantify joint SRS in concentric loading conditions where active muscles were shortened. For eccentric loading it was shown that SRS increases proportionally with joint torque (Cui et al., 2007; van Eesbeek et al., 2010) and that EL increased proportionally with lengthening velocity (Campbell et al., 2003; de Vlugt et al., submitted).

The purpose of this study was to estimate SRS and EL for concentric loading and to compare joint SRS and EL to those obtained for eccentric wrist loading. A previous developed method was used to identify SRS and EL from in vivo recordings of the human wrist joint. Results are discussed in relation to contractile properties of cross-bridges and possible clinical applications.

2 Method

The instrumentation and identification method to estimate joint SRS was described in detail in (van Eesbeek et al., 2010) and described here in brief.

2.1 Instrumentation

Ramp-and-Hold (RaH) flexion and extension rotations of 0.15 rad were imposed to the wrist joint by an electrical motor, controlled as a stiff servo (1000 Nm/rad) (Schouten et al., 2006). The wrist flexion-.

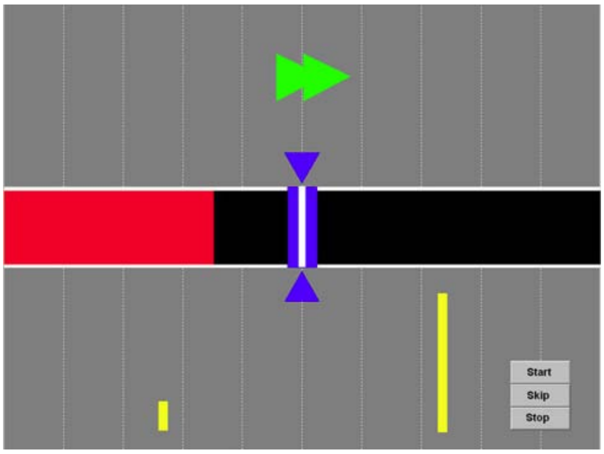

Fig. 1. Left: Top view of the experimental setup (see Text). Right: Display for visual feedback to the subject. Wrist flexion torque was visualized by a moving horizontal red bar that emerged from the left. Green arrows indicated the direction of wrist torque to be requested from the subject. Target torque range was indicated by the blue area (± 2.5 % of target torque level). Flexor and extensor muscle activity was displayed by vertical yellow bars (left and right respectively) of which the height was proportional to the EMG (normalized to MVC) of the corresponding muscles and used to minimize co-contraction.

extension axis was aligned to the axis of the motor Angular displacement was measured by a digital encoder. Torque exerted at the wrist was measured by strain gauges within the lever arm of the motor.

Activity of the wrist flexor carpi radialis (FCR) and the wrist extensor carpi radialis (ECR) was recorded by bi-polar surface EMG (Delsys Bagnoli-4, 20–450Hz bandpass, 10mm inter-electrode distance), full-wave rectified and used to monitor eventual co-contraction and reflex activity. All signals were sampled at 5 kHz and low-pass filtered (50 Hz, 3rd order Butterworth).

The wrist was aligned with the axis of the actuated lever and the forearm and hand were fixated such that only flexion and extension movement of the wrist was possible. The elbow was immobilized at the lateral and medial epicondyles of the humeral bone by clamps with a stiff rubber interface (Fig. 1, Left). Clamps in combination with individually fitted polypropylene (PP) foam malls were used at the styloid processes of the radial and ulnar to fixate the wrist. The hand was fixated to the handle by an individually molded PP foam mall, which was placed over the metacarpo-phalangeal joints using tie wraps.

2.2 Experimental protocol

A group of nine volunteers (26 ± 2years, four male) participated in the study and signed informed consent. Subjects were instructed to generate different target levels of flexion torque being 0, 0.6, 1.2 and 1.8Nm.

RaH rotations at three velocities (0.65, 1.95 and 3.25rad/s) were applied in either flexion or extension direction, inducing the active flexor muscles to be shortened (concentric loading) or lengthened (eccentric loading) respectively. RaH movement was applied when wrist torque was within ± 2.5 % of target torque level for 0.5s. All combinations of three velocities and four joint torques were applied three times and in a random order. A 15 s period of rest was included after each perturbation to prevent fatigue and possible effects on SRS from previous RaH movement (Campbell and Moss, 2002). Visual task feedback was provided on a computer screen in front of the subject (Fig. 1, Right). To minimize co-contraction, the magnitude of the filtered EMG of the flexor and extensor muscles were also visualized on the same computer screen during the execution of the tasks (Fig. 1, Right). The total of 72 trials (4 torque levels, 3 velocities, 2 directions, 3 repetitions) had a total duration of less than 30 minutes.

2.3 Impedance model

A dynamic nonlinear model was used to estimate SRS (Fig. 3). The model was expressed in the angular domain. No attempt was made to discriminate into individual contributions of muscles and tendons.

The model consists of three pairs of spring-damper elements separated by two inertial loads; I_l is the lever inertia and I_j the inertia of the wrist joint. Subsystem I includes the stiffness, k_l, and damping, b_l, of the lever compliance. Subsystem II includes the elasticity, k_h, and viscosity, b_h, of the hand–handle interface. Subsystem III includes the elasticity, k_j, and viscosity, b_j, of the muscle–tendon units. The spring k_j was designed as a nonlinear bi-phasic stiffness component

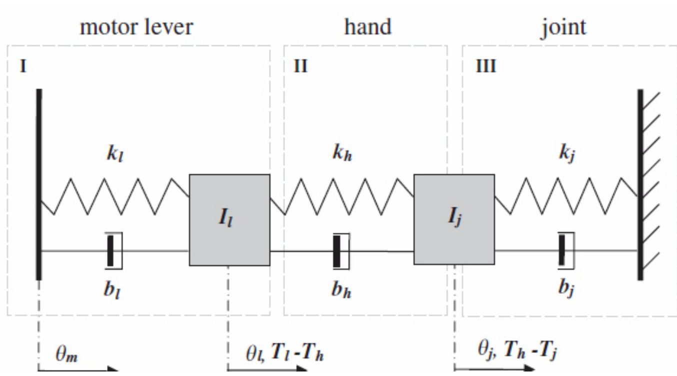

Fig. 2, Schematic presentation of the dynamic model used for parameter estimation. The model was expressed in the '*angular*' domain **and includes two inertial loads I_l and I_j, representing the inertia of the lever plus handle and the human wrist joint respectively. The inertias were separated by three visco-elastic compartments, being: I, the motor lever (indexed by *l*); II, the hand tissues (indexed by *h*); III, the joint (indexed by *j*). Viscous elements are indicated by *b*, stiffness elements by *k*, angles by θ_m, θ_l, and θ_j for the motor axis, lever handle and wrist joint respectively and torque by T_l, T_h and T_j for the lever, hand and the joint respectively. T_l and θ_m were available from recordings.**

$$k_j = \begin{cases} k_{srs} & \theta_j < x_e \\ k_{srs} - k_{dec} & \theta_j > x_e \end{cases} \tag{1}$$

with k_{srs} the joint SRS, x_e the elastic limit and k_{dec} the decrease in SRS beyond x_e. The stiffness component is implemented in the model by a logarithmic torque-angle function (Fig. 3):

$$T_{j,elas} = k_{srs}\theta_j - \log\left[1 + \exp\left(a_s \cdot k_{dec} \cdot \left(\theta_j - x_e\right)\right)\right] / a_s \tag{2}$$

with $T_{j,elas}$ the elastic joint torque and a_s= 100 a fixed smoothness parameter for the stiffness transition at x_e. Stiffness beyond the EL was taken as $k_{after} = k_{srs} - k_{dec}$. The complete model is expressed by the following set of differential equations:

$$I_l\ddot{\theta}_l = \left(\dot{\theta}_m - \dot{\theta}_l\right)b_l + \left(\theta_m - \theta_l\right)k_l - \left(\dot{\theta}_l - \dot{\theta}_j\right)b_h + \left(\theta_l - \theta_j\right)k_h \tag{3}$$

$$I_j\ddot{\theta}_j = \left(\dot{\theta}_l - \dot{\theta}_j\right)b_j + \left(\theta_l - \theta_j\right)k_j - \dot{\theta}_j b_j - \theta_j k_j \tag{4}$$

2.4 Data analysis

The model parameters were estimated by minimization of the quadratic difference between the measured (T_l) and the predicted torque on the handle ($\hat{T}_l$). Torque and angle just before the start of the RaH movement ($t=t_0$) were defined as y_0 and T_0, respectively, and were subtracted from the corresponding traces as the model only describes changes w.r.t. steady state. To avoid variation in muscle force from stretch reflexes, a 50 ms time interval from the start of the RaH movement was taken for parameterization. The model was implemented in Simulink and the optimization was performed in Matlab (The Mathworks Inc.) using a nonlinear gradient search algorithm.

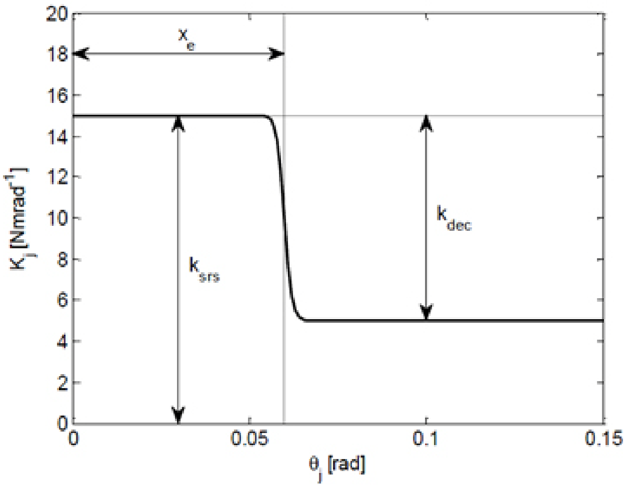

Fig. 3, Stiffness profile of the nonlinear spring as used to describe the joint stiffness: x_e represents the elastic limit, marking the angle of stiffness reduction k_{dec} from the short range stiffness k_{srs} to the stiffness beyond the elastic limit.

Model parameters for lever inertia, stiffness and damping (I_l, k_l, b_l) were taken from (van Eesbeek et al., 2010) and kept constant throughout all optimizations. Joint damping, b_j, appeared to have a negligible effect on the predicted torque, $\hat{T}_l$, and was therefore fixed at a small value (10^{-5} Nm s/rad) to provide numerical stability. For each subject a total of six parameters (I_j, b_h, k_h, k_{srs}, k_{dec}, x_e) were estimated simultaneously for all conditions and repeated for each repetitions. I_j was constrained to be identical for all conditions within each individual subject. The model fit was validated by the Variance Accounted For (VAF)

$$VAF = 1 - \frac{\sum_{i=1}^{n}\left(\theta_{m,i} - \hat{\theta}_{m,i}\right)^2}{\sum_{i=1}^{n}\left(\theta_{m,i}\right)^2} \tag{5}$$

where i indexes the time sample, n = 250 the number of data points, $\theta_{m,i}$ the measured and $\hat{\theta}_{m,i}$ the modeled motor angle. Parameter reliability was indicated by the Standard Error of the Mean (SEM):

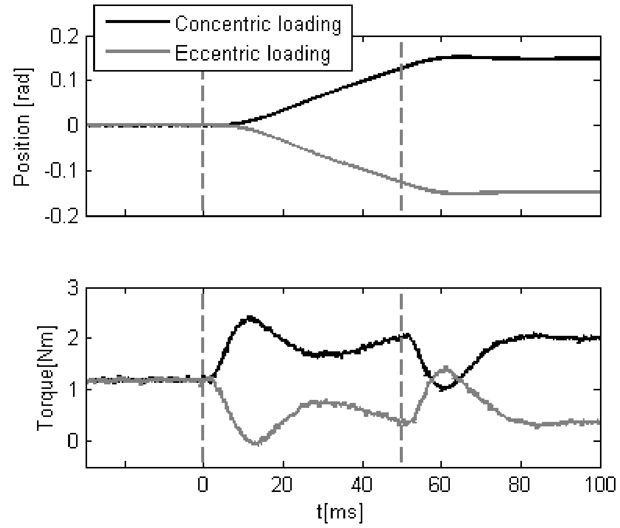

Fig. 4, Typical position and torque recordings of the handle for a subject (*T0* = 1.2 Nm, 1.95 rad / s) at expanded time axes. A: measured angle. B: measured torque. Dotted lines denote the 50 ms time window used for parameterization of the model**.**

$$SEM = \sqrt{\frac{1}{n} I \left(J^T J\right)^{-1} \sum_{i=1}^{n} \left(E_i\right)^2} \tag{6}$$

with $E_i = T_{l,i} - \hat{T}_{l,i}$, the error of the fit, *J* is the Jacobian (*n* x n_p vector of first derivatives of the error to each parameter, with n_p = 6 the number of parameters), and I the identity matrix. Eq. 6 produces a vector of n_p SEM-values for each optimized model parameter. The SEM equals the deviation of the parameter to its theoretical value at the minimal (optimal) error. SEM was normalized to the corresponding parameter value. A General Linear Model repeated measurements ANOVA was used to test the effect of torque, velocity and direction on the estimated model parameters using SPSS at an alpha of 0.05.

3 Results

Fig. 4 shows typical recordings of the lever angle and torque. The time used for identification (50 ms) is indicated by the dotted lines. Fig. 5 shows a typical result of the measured and predicted torque on the handle.

For all subjects and all conditions, the model was able to describe the recorded torque accurately with VAF values higher than 0.998 and SEM values of 0.0238.

3.1 Eccentric versus concentric loading

Fig. 6 shows all model parameters against torque for eccentric and concentric loading conditions, averaged over subjects and trials. The decrease in stiffness beyond SRS, k_{dec}, was higher for concentric loading

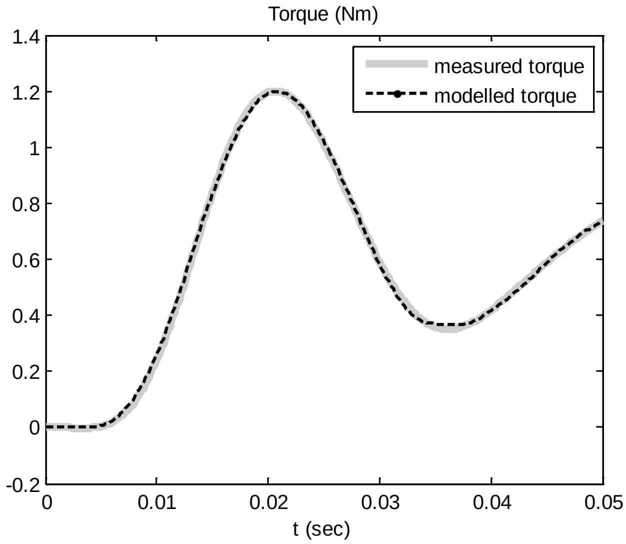

Fig. 5, Typical example of recorded and predicted torque.

(p=0.048, F=5.42). For all other model parameters, including SRS and EL, no significant differences were found between eccentric and concentric loading for all torque levels and velocities.

3.2 Variation with Torque

SRS increased with joint torque from 5.9 Nm/rad at the lowest to 14 Nm/rad at the highest torque level ($p<0.001$, F = 70.29). EL decreased with torque (p=0.034, F = 5.91). The decrease in stiffness beyond SRS, k_{dec} increased with torque ($p<0.001$ F = 26.66). The slope by which SRS increased with torque had mean values of α_{ecc}= 6.01/rad for eccentric direction and α_{con}= 6.42/ rad for concentric direction.

3.3 Variation with Velocity

The EL increased with velocity ($p<0.001$, F =194.24) (Fig. 6). SRS and the decrease in stiffness after SRS, k_{dec} did not change significantly with velocity.

4 Discussion

The goal of this study was to identify SRS in concentric conditions and to compare the results to eccentric conditions. SRS, EL and the decrease in stiffness beyond SRS, k_{dec} were estimated from in vivo recordings of wrist torque and angle. Results showed that SRS and EL in concentric loading did not differ from eccentric loading conditions. The decrease in stiffness beyond the EL, k_{dec}, was larger for concentric compared to eccentric condition.

4.1 SRS and EL in concentric loading

Elastic behavior was examined during brief ramp and

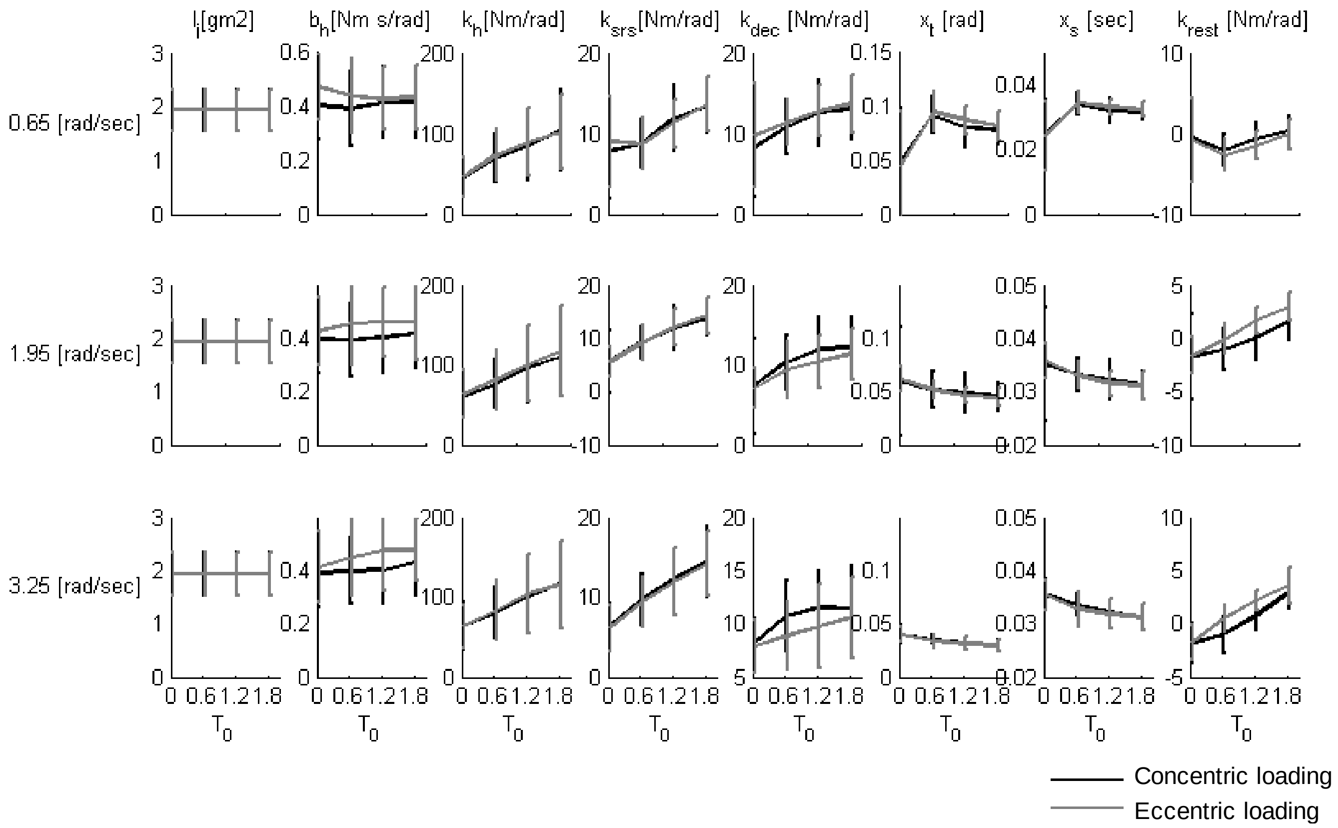

Fig. 6, Estimated model parameters averaged over all subjects and observations (mean ± 1 s. d.) for the three movement velocities (upper, middle and bottom row), eccentric and concentric direction (grey and black) and the four incremented torque levels (horizontal axes). The SRS period, x_t, was derived from the estimated parameters and the model simulation and taken as the elapsed time from the onset of the RaH to the time instance where the (simulated) joint angle was equal to the elastic limit. The stiffness beyond the elastic limit, k_{after} (bottom row), was taken equal to $k_{srs} - k_{dec}$.

hold (RaH) movements applied in both flexion and extension direction. For both movement directions the data were well described by the same model structure. We conclude that SRS behavior was similar for both directions of movement. Corresponding results were found in experiments on fiber (Campbell and Lakie, 1998; Roots et al., 2007) as well as on muscle level (Herzog and Leonard, 1997; Joyce et al., 1969; Rack and Westbury, 1974). Although this muscle behavior was not referred to SRS by the authors, it indicated a high stiffness at the start of a movement and less stiffness thereafter.

4.2 Decrease in stiffness after SRS

The decrease in stiffness beyond the EL, k_{dec} was found to be larger in concentric compared to eccentric loading. This difference increased with velocity (Fig. 7) but not significantly.

It is well known from the force velocity relationship of active muscle that muscle force decreases exponentially as the velocity of shortening increases (Hills, 1938). In contrast, when a muscle is actively lengthened, the force developed by the muscle increases with increasing speeds of lengthening. In a study by (Roots et al., 2007) on intact muscle fibers, Hills force velocity relation was reproduced by applying ramp shortening and lengthening movements at different velocities. The tension at the break point of the length tension response corresponds with EL in this study, was plotted against the velocity of shortening or lengthening providing the same relation as in Hill.

Similar as in (Roots et al., 2007) the force velocity relation obtained in this study can be calculated on fiber level. Velocity at human optimal fiber length is expressed as:

$$v_f = \frac{v_j \cdot r}{l_f} \tag{7}$$

where v_f and v_j are velocities on optimal fiber length (l_0) and joint level respectively, r is the human moment arm of the wrist and l_0 is the optimum fiber length. Given the mean human fiber length of human wrist flexor muscles as obtained from (Lieber et al., 1990; Lieber et al., 1992) and the mean wrist flexor muscles moment arm (Ramsay et al., 2009) the velocities used in this study of

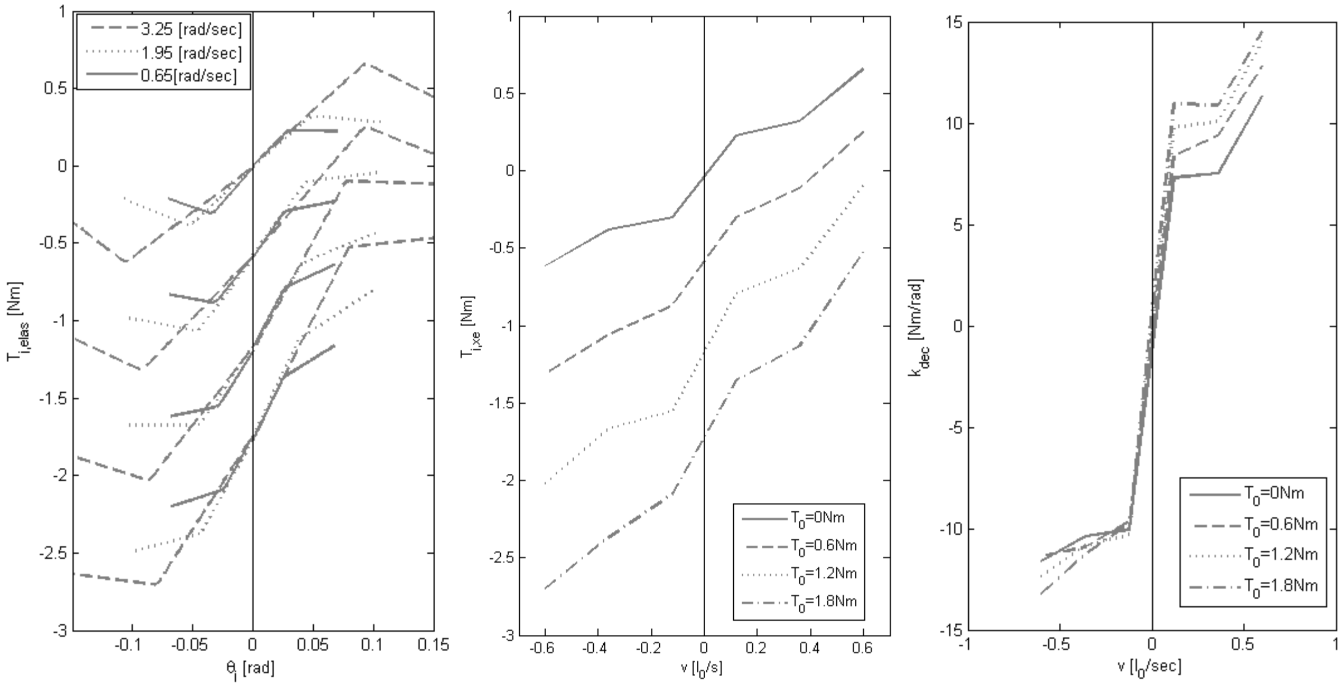

Fig. 7, Typical model predictions of the elastic muscle–tendon wrist torque and k_{dec}. Left: elastic torque ($T_{j,elas}$) against muscle-tendon lengthening as described by the joint angle θ_j. for the three movement velocities. Concentric and eccentric loading is shown at $-\theta$ and $+\theta$ respectively. Negative elastic torque ($T_{j,elas}$) implicates a torque in flexion direction of the wrist. Middle: torque at the elastic limit, x_e against the shortening and lengthening velocity at the optimal fiber length, (l_0*/sec*) for the four incremented torque levels . Right: k_{dec} against the shortening and lengthening velocity at the optimal fiber length, (l_0*/sec*) for the four incremented torque levels.

0.12 l_0/s respectively. The force velocity relation obtained in this study is visualized (Fig. 7, middle), where the torque at the EL, x_e is plotted against the velocity at the optimal fiber length, l_0 per second (negative values indicate to shortening). The slope of the second part of the torque-angle relation (Fig. 7, left) increases with lengthening velocity and reversely changes with shortening velocity (Fig. 7, right). Compared to (Roots et al., 2007) velocities used in this study are relatively low. The lengthening velocities used in this study are within the region where an increase of tension upon lengthening velocity is found in (Roots et al., 2007). Results of this study also show an increase of torque with lengthening velocity. The shortening velocities used here are within the region where tension decreases fast with an increase in shortening velocity although a decrease in torque with shortening velocity is found in this study it seems to be slower than found in (Roots et al., 2007).

4.3 Implication

For muscle shortening as well as muscle lengthening SRS in found to be present in small movements. When rotating a joint the agonist is lengthened while the antagonist is obviously shortened. Consequently, during measurements on joint level both eccentric and concentric loading will be present. The existence of SRS in both directions implicates that a distinction can be made in active and passive contribution on joint level during joint rotations, assuming that stiffness of passive tissue does not change with force.

4.4 Future research

Since results of this study showed that SRS is also present and increasing with activation in the shortening muscle, it is showed that the contribution to joint stiffness of all involved cross bridges can be distinguished from passive structures in concentric loading. Future research on co-contracted joints can be performed where activated muscles are either shortened or lengthened, which is important for studying the control of joint mobility (net torque) and stability (stiffness) on joint level. This creates the possibility to do measurements in patients suffering from movement disorders, where high joint stiffness is reported.

5 Conclusion

SRS is equal in concentric and eccentric loading which shows that cross-bridge behavior is elastic in both directions for small and rapid movements.

The decrease in stiffness after SRS, k_{dec} is greater in concentric loading compared to eccentric loading. The results corresponded well to the muscle force velocity relation.

Discrimination of active from passive and reflexive stiffness is now also possible in concentric loading, creating the possibility to allocate the high stiffness found in movement disorders in joint measurements. This technique is expected to be important for clinical purpose especially in movement disorders where the active muscle components are affected.

References

Campbell KS, Lakie M. 1998. A cross-bridge mechanism can explain the thixotropic short-range elastic component of relaxed frog skeletal muscle. Journal of Physiology-London 510:941-962.

Campbell KS, Moss RL. 2002. History-dependent mechanical properties of permeabilized rat soleus muscle fibers. Biophysical Journal 82:929-943.

Campbell KS, Patel JR, Moss RL. 2003. Cycling cross-bridges increase myocardial stiffness at submaximal levels of Ca2+ activation. Biophysical Journal 84:3807-3815.

Cui L, Perreault EJ, Sandercock TG. 2007. Motor unit composition has little effect on the short-range stiffness of feline medial gastrocnemius muscle. Journal of Applied Physiology 103:796-802.

de Vlugt E, van Eesbeek S, Baines P, Hilte J, Meskers CGM, de Groot JH. Short Range Stiffness Elastic Limit Depends on Joint Velocity. In. submitted.

Herzog W, Leonard TR. 1997. Depression of cat soleus forces following isokinetic shortening. Journal of Biomechanics 30:865-872.

Joyce GC, Rack PMH, Westbury DR. 1969. Mechanical Properties of Cat Soleus Muscle During Controlled Lengthening and Shortening Movements. Journal of Physiology-London 204:461-&.

Lieber RL, Fazeli BM, Botte MJ. 1990. Architecture of Selected Wrist Flexor and Extensor Muscles. Journal of Hand Surgery-American Volume 15A:244-250.

Lieber RL, Jacobson MD, Fazeli BM, Abrams RA, Botte MJ. 1992. Architecture of Selected Muscles of the Arm and Forearm - Anatomy and Implications for Tendon Transfer. Journal of Hand Surgery-American Volume 17A:787-798.

Petit J, Filippi GM, Emonetdenand F, Hunt CC, Laporte Y. 1990. Changes in Muscle-Stiffness Produced by Motor Units of Different Types in Peroneus Longus Muscle of Cat. Journal of Neurophysiology 63:190-197.

Rack PM, Westbury DR. 1974. The short range stiffness of active mammalian muscle and its effect on mechanical properties. J. Physiol 240:331-350.

Ramsay JW, Hunter BV, Gonzalez RV. 2009. Muscle moment arm and normalized moment contributions as reference data for musculoskeletal elbow and wrist joint models. Journal of Biomechanics 42:463-473.

Roots H, Offer GW, Ranatunga KW. 2007. Comparison of the tension responses to ramp shortening and lengthening in intact mammalian muscle fibres: crossbridge and non-crossbridge contributions. Journal of Muscle Research and Cell Motility 28:123-139.

Schouten AC, de Vlugt E, van Hilten JJB, van der Helm FCT. 2006. Design of a torque-controlled manipulator to analyse the admittance of the wrist joint. Journal of Neuroscience Methods 154:134-141.

van Eesbeek S, de Groot JH, van der Helm FC, de Vlugt E. 2010. In vivo estimation of the short-range stiffness of cross-bridges from joint rotation. J. Biomech. 43:2539-2547.

Walmsley B, Proske U. 1981. Comparison of stiffness of soleus and medial gastrocnemius muscles in cats. J. Neurophysiol. 46:250-259.

Short Range Stiffness During Voluntary Contraction

Thesis

Ilse van der Greft

April 2011

TU Delft Delft University of Technology

LUMC Leiden University Medical Center

1 Introduction

The stabilizing behavior of a joint is determined by its visco-elastic properties. At the department of Biomechanical Engineering at Delft University of Technology (DUT) and the department of Rehabilitation Medicine at Leiden University Medical Center (LUMC), research is being performed to understand the regulation of human joint visco-elastic properties.

In a study on joint rotation, performed by van Eesbeek (2010), it was observed that stiffness of a joint is high at the start of the rotation and drops at a certain angle. This bi-phasic force response is also found in several other studies on muscle level (Cui et al., 2007; Joyce et al., 1969; Petit et al., 1990; Rack and Westbury, 1974; Walmsley and Proske, 1981) and muscle fiber level (Campbell and Lakie, 1998). The high initial force response is referred to as Short Range Stiffness (SRS) and the moment at which the force response drops is referred to as the elastic limit (EL). It is likely that this bi-phasic torque response is caused by the properties of the contractile elements of the muscle. The first part of the force response is attributed to the elastic stretch of attached cross-bridges and the stiffness reduction is attributed to the breakage of cross bridges.

SRS is dependent on activation level; with higher activation SRS increases (Cui et al., 2007; van Eesbeek et al., 2010). EL increases proportionally with lengthening velocity (Campbell et al., 2003; de Vlugt et al., submitted). SRS provides a measure by which the contribution of the active muscle components can be separated from the passive components, which stiffness contribution does not show a bi-phasic pattern with a muscle stretch. In research, joint properties in humans are typically measured during continues movements in both flexion and extension direction. When a joint is rotated, the agonists is lengthened and consequently, the antagonist will always be shortened, and vice versa. To date detailed studies focusing on SRS have been performed only for lengthening of muscles (eccentric loading). In case of co-contraction, when both agonistic and antagonistic muscles are activated, joint torque and stiffness are no longer uniquely related, as is the case for unilateral contraction. During co-contraction measurements on joints both eccentric and concentric loading will be present. Consequently, the existence of SRS in concentric loading needs to be studied in order to indicate whether the SRS-torque relation counts for concentric loading. A previous developed identification procedure was used to identify SRS and EL in concentric condition from in vivo recordings of the human wrist joint. This identification procedure is characterized by a non linear spring, indicating the transition between high (SRS) and low (k_{rest}) stiffness. The curvature that describes the transition between SRS and k_{rest} . Another characteristic of this method is its relatively short time frame which was used for identification in order to avoid variation in muscle activity from stretch reflexes. To verify the characteristics of the identification procedure, the curvature of the transition between SRS and k_{rest} and the used time frame was tested.

In this study a method to quantify co-contraction has been proposed based on SRS properties for eccentric and concentric loading. Results of this study can be used in future research on movement disorders as in e.g. stroke were a higher joint stiffness is often observed (Burne et al., 2005; Meskers et al., 2009; Mirbagheri et al., 2001) of which the origin may be due to increased levels of muscle (co-)contraction (Burne et al., 2005). Alternatively, increased joint stiffness in patients may also result from altered properties of passive tissues (connective, tendinous, ligamentous) or from stretch reflexes.

In the elderly, loss of muscle force and a loss of contractile speed are reported. Possible reasons for this loss are a decline in number of excitable motor units, a loss of type II muscle fibers, an increased level of fat and connective tissue, a reduced activity in the sarcoplasmic reticulum whitin the muscle, altered moment arms and fiber pennation angle (Ramamurthy et al., 2003; Vandervoort, 2002). Studies on skinned fibers and single motor units have indicated that slow-twitch fibers are stiffer than fast-twitch fibers (Malamud et al., 1996). The many changes occurring in aging muscles may alter the stiffness properties of the joint. The SRS method used in this study could indicate whether the contractile elements in the muscle has the highest contribution to the altered joint properties.

The aim of this study was to examine the effect of muscle shortening (concentric loading) on SRS and EL in young and elderly subjects and to test the curvature of the transition between SRS and k_{rest} and the used time frame of the identification method in order to develop a method to quantify co-contraction.

Chapter 2 provides a description and a test of the SRS estimation method. Chapter 3 provides 1) the results of the main study (in a scientific paper format) where SRS properties during concentric loading conditions were compared to similar eccentric loading conditions, 2) a first application of the results to estimate co-contraction and 3) the results of the measurements on elderly subjects. In Chapter 4 the results are discussed in relation to cross-bridge physiology and also possible clinical applications are sketched.

2 Method

The instrumentation and identification method to estimate joint SRS was described in detail in (van Eesbeek et al., 2010) and described here in brief.

2.1 Instrumentation

Ramp-and-Hold (RaH) flexion and extension rotations of 0.15 rad were imposed to the wrist joint by an electrical motor, controlled as a stiff servo (1000 Nm/rad) (Schouten et al., 2006). The wrist flexion-extension axis was aligned to the axis of the motor. Angular displacement was measured by a digital encoder. Torque exerted at the wrist was measured by strain gauges within the lever arm of the motor.

Activity of the wrist flexor carpi radialis (FCR) and the wrist extensor carpi radialis (ECR) was recorded by bi-polar surface EMG (Delsys Bagnoli-4, 20–450Hz bandpass, 10mm inter-electrode distance), full-wave rectified and used to monitor eventual co-contraction and reflex activity. All signals were sampled at 5 kHz and low-pass filtered (50 Hz, 3rd order Butterworth).

The wrist was aligned with the axis of the actuated lever and the forearm and hand were fixated such that only flexion and extension movement of the wrist was possible. The elbow was immobilized at the lateral and medial epicondyles of the humeral bone by clamps with a stiff rubber interface (Fig. 1, Left). Clamps in combination with individually fitted polypropylene (PP) foam malls were used at the styloid processes of the radial and ulnar to fixate the wrist. The hand was fixated to the handle by an individually molded PP foam mall, which was placed over the metacarpo-phalangeal joints using tie wraps.

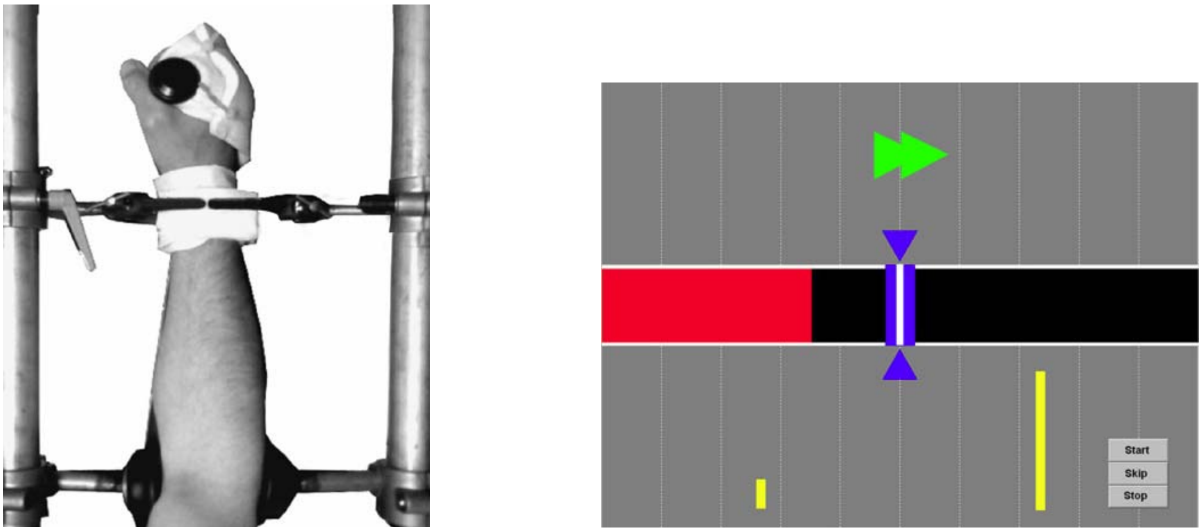

Fig. 1. Left panel: Top view of the experimental setup (see Text). Right panel: Display for visual feedback to the subject. Wrist flexion torque was visualized by a moving horizontal red bar that emerged from the left. Green arrows indicated the direction of wrist torque to be requested from the subject. Target torque range was indicated by the blue area (± 2.5 % of target torque level). Flexor and extensor muscle activity was displayed by vertical yellow bars (left and right respectively) of which the height was proportional to the EMG (normalized to MVC) of the corresponding muscles and used to minimize co-contraction.

2.2 Experimental protocol

A group of nine young volunteers (26 ± 2years, four male) and a group of 6 elderly volunteers (62 ± 2 years, 4 male) participated in the study and signed informed consent. Subjects were instructed to generate different target levels of flexion torque being 0, 0.6, 1.2 and 1.8Nm.

RaH rotations at three velocities (0.65, 1.95 and 3.25rad/s) were applied in either flexion or extension direction, inducing the active flexor muscles to be shortened (concentric loading) or lengthened (eccentric loading) respectively. RaH movement was applied when wrist torque was within ± 2.5 % of target torque level for 0.5s. All combinations of three velocities and four joint torques were applied three times and in a random order. Visual task feedback was provided on a computer screen in front of the subject (Fig. 1, Right). A 15s period of rest was included after each perturbation to prevent fatigue and possible effects on SRS from previous RaH movement (Campbell and Moss, 2002). To minimize co-contraction, the magnitude of the filtered EMG of the flexor and extensor muscles were visualized on the computer screen during the execution of the tasks. The total of 72 trials (4 torque levels, 3 velocities, 2 directions, 3 repetitions) had a total duration of less than 30 minutes.

Co-contraction

Co-contraction was initiated by the use of combinations of torque and EMG levels. Activation of the agonist was achieved by exerting a torque to the handle. A constant activation level of the antagonist was achieved by keeping EMG on a specified level. A RAH rotation was induced when the requested torque-EMG combination was met. Participants were asked to generate torques between 0Nm and 1.8Nm. EMG levels for the antagonist were determined by measuring the EMG at a torque of 0Nm and 2Nm. The activation level of the antagonist was obtained from the EMG level at the 0Nm torque and 15%, 30%, 45% and 60% of the EMG level of the 2Nm torque. Visualization of the task was given on a screen in front of the participant (Fig. 2). The rotating white bar represents the amount and direction of the torque on the handle. The blue bar represents the amount of EMG of the antagonist and slides along the white bar. The green dot is the target EMG and torque level.

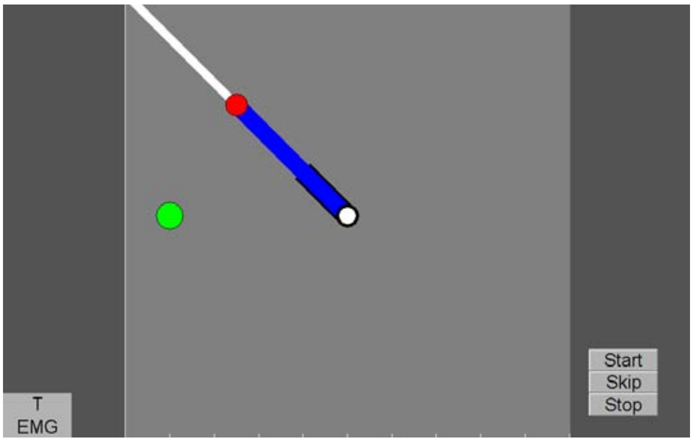

Fig. 2, Display for visual feedback to the subject, for the co-contraction measurements. The rotating white bar represents the amount and direction of the torque on the handle. The blue bar represents the amount of EMG of the antagonist and slides along the white bar. The green dot is the target EMG and torque level.

2.3 Impedance model

To estimate SRS a dynamic nonlinear model was used (Fig. 3). The model was expressed in the angular domain. No attempt was made to discriminate into individual contributions of muscles and tendons (van Eesbeek et al., 2010).

The model consists of three pairs of spring-damper elements separated by two inertial loads; I_l is the lever inertia and I_j the inertia of the wrist joint. Subsystem I includes the stiffness, k_l, and damping, b_l, of the lever compliance. Subsystem II includes the elasticity, k_h, and viscosity, b_h, of the hand–handle interface. Subsystem III includes the elasticity, k_j, and viscosity, b_j, of the muscle–tendon units. The spring k_j was designed as a nonlinear bi-phasic stiffness component

$$k_j = \begin{cases} k_{srs} & \theta_j < x_e \\ k_{srs} - k_{dec} & \theta_j > x_e \end{cases} \tag{1}$$

with k_{srs} the joint SRS, x_e the EL and k_{dec} the decrease in SRS beyond x_e. The stiffness component is implemented in the model by a logarithmic torque-angle function (Fig. 3):

$$T_{j,elas} = k_{srs}\theta_j - \log\left[1+\exp\left(a_s \cdot k_{dec} \cdot \left(\theta_j - x_e\right)\right)\right] / a_s \qquad (2)$$

with $T_{j,elas}$ the elastic joint torque and a_s= 100 a fixed smoothness parameter for the stiffness transition at x_e. Stiffness beyond the EL was taken as k_{after} = k_{srs} – k_{dec}. The complete model is expressed by the following set of differential equations:

$$I_l\ddot{\theta}_l = \left(\dot{\theta}_m - \dot{\theta}_l\right)b_l + \left(\theta_m - \theta_l\right)k_l - \left(\dot{\theta}_l - \dot{\theta}_j\right)b_h + \left(\theta_l - \theta_j\right)k_h \qquad (3)$$

$$I_j\ddot{\theta}_j = \left(\dot{\theta}_l - \dot{\theta}_j\right)b_j + \left(\theta_l - \theta_j\right)k_j - \dot{\theta}_j b_j - \theta_j k_j \qquad (4)$$

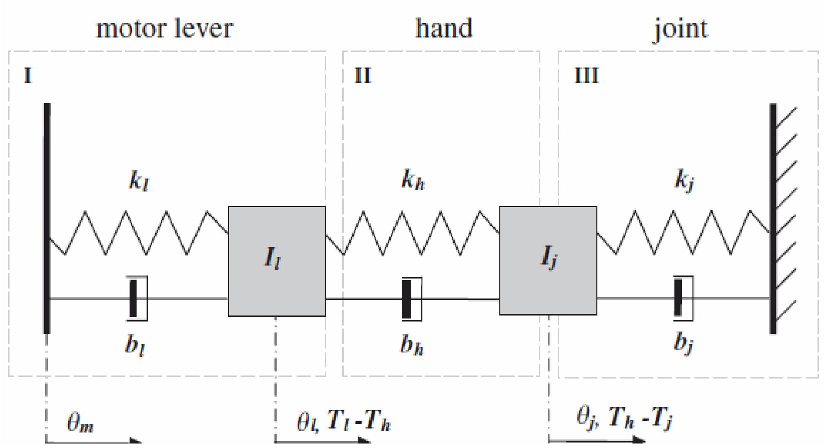

Fig. 3, Schematic presentation of the dynamic model used for parameter estimation. The model was expressed in the '*angular*' domain and includes two inertial loads I_l and I_j, representing the inertia of the lever plus handle and the human wrist joint respectively. The inertias were separated by three visco-elastic compartments, being: I, the motor lever (indexed by *l*); II, the hand tissues (indexed by *h*); III, the joint (indexed by *j*). Viscous elements are indicated by *b*, stiffness elements by *k*, angles by ϑ_m, ϑ_l, and ϑ_j for the motor axis, lever handle and wrist joint respectively and torque by T_l, T_h and T_j for the lever, hand and the joint respectively. T_l and ϑ_m were available from recordings.

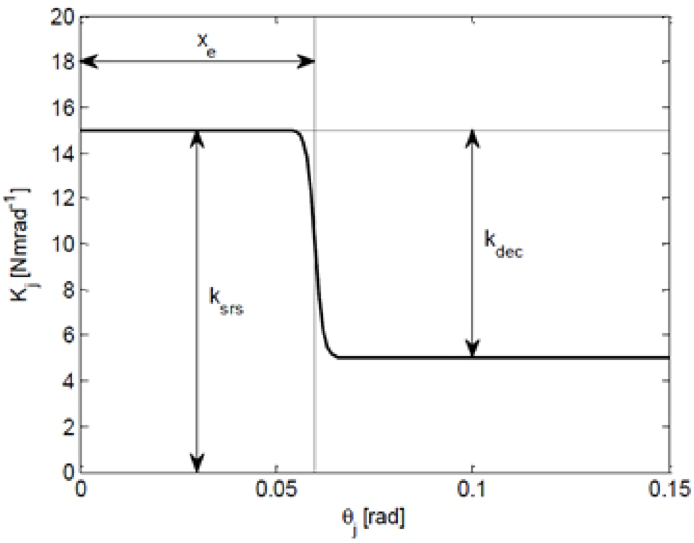

Fig. 4, Stiffness profile of the nonlinear spring as used to describe the joint stiffness: xe represents the elastic limit, marking the angle of stiffness reduction kdec from the short range stiffness ksrs to the stiffness beyond the elastic limit.

2.4 Data analysis

The model parameters were estimated by minimization of the quadratic difference between the measured (T_l) and the predicted torque on the handle ($\hat{T}_l$). Torque and angle just before the start of the RaH movement ($t=t_0$) were defined as y_0 and T_0, respectively, and were subtracted from the corresponding traces as the model only describes changes w.r.t. steady state. To avoid variation in muscle activity from stretch reflexes, a 50 ms time interval from the start of the RaH movement was taken for parameterization. The model was implemented in Simulink and the optimization was performed in Matlab (The Mathworks Inc.) using a nonlinear gradient search algorithm.

Model parameters for lever inertia, stiffness and damping (I_l, k_l, b_l) were taken from (van Eesbeek et al., 2010) and kept constant throughout all optimizations (I_l=0.0015kgm^2, k_l=2570Nm/rad, b_l=0.14Nm/rad/sec). Joint damping, b_j, appeared to have a negligible effect on the predicted torque, $\hat{T}_l$, and was therefore fixed at a small value (10^{-5} Nm s/rad) to provide numerical stability. For each subject a total of six parameters (I_j, b_h, k_h, k_{srs}, k_{dec}, x_e) were estimated simultaneously for all conditions and repeated for each repetitions. I_j was constrained to be identical for all conditions within each individual subject. The model fit was tested by the Variance Accounted For (VAF)

$$VAF = 1 - \frac{\sum_{i=1}^{n}\left(\theta_{m,i} - \hat{\theta}_{m,i}\right)^2}{\sum_{i=1}^{n}\left(\theta_{m,i}\right)^2} \tag{5}$$

where i indexes the time sample, n = 250 the number of data points, $\theta_{m,i}$ the measured and $\hat{\theta}_{m,i}$ the modeled motor angle. Parameter reliability was indicated by the Standard Error of the Mean (SEM):

$$SEM = \sqrt{\frac{1}{n} I \left(J^T J\right)^{-1} \sum_{i=1}^{n}\left(E_i\right)^2} \tag{6}$$

with $E_i = T_{l,i} - \hat{T}_{l,i}$, the error of the fit, J is the Jacobian (n x n_p vector of first derivatives of the error to each parameter, with n_p = 6 the number of parameters), and I the identity matrix. Eq. 6 produces a vector of n_p SEM- values for each optimized model parameter. The SEM equals the deviation of the parameter to its theoretical value at the minimal (optimal) error. SEM was normalized to the corresponding parameter value. A General Linear Model repeated measurements ANOVA was used to test the effect of torque, velocity and direction on the estimated parameters using SPSS at an alpha of 0.05.

2.5 Time frame

In a previous study by van Eesbeek (2010) a time frame of 40ms was taken for the optimization procedure to estimate the model parameters. Here a time frame was chosen for future identification by estimating all parameters at a time frame of 40 to 70ms and testing the reliability of the fit with the use of VAF en SEM values.

2.6 Stiffness curvature

The curvature of the transition between the SRS and k_{dec} is described by one parameter a_s (2). Fig. 5 (left) shows the force response of the nonlinear spring, as used to describe the joint stiffness, when a_s is adjusted to values between $a_s=10^0$ and $a_s=10^3$. Corresponding stiffness of the spring is shown in Fig. 5 (right). The influence of the shape of the curvature to the optimization was examined by identifying measurements for $10^0 \leq a_s \geq 10^{2.5}$ and test the reliability of the fit with the use of VAF and SEM values.

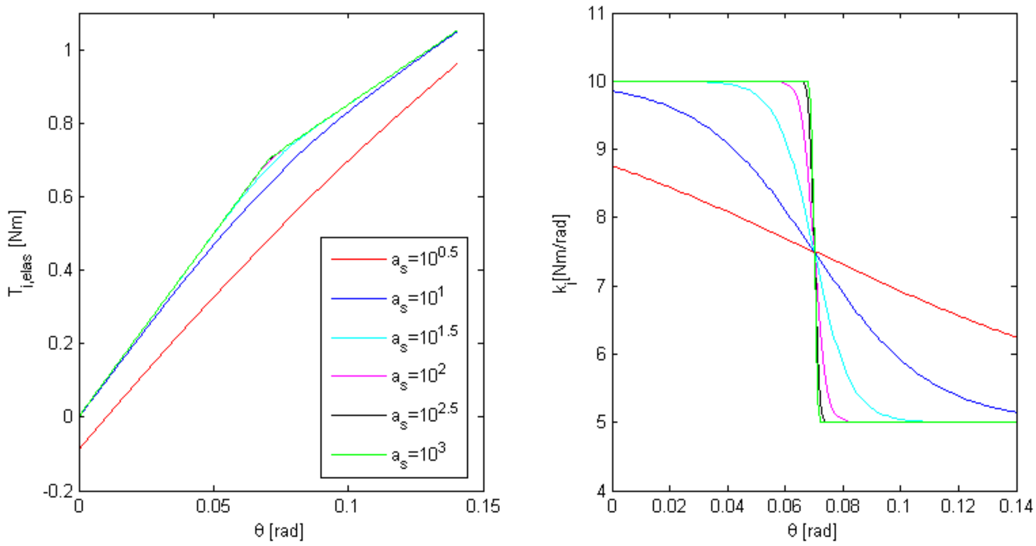

Fig. 5, Model predictions of elastic muscle–tendon wrist torque and stiffness at several values of as. Left panel: elastic torque (Tj,elas) as function of angle(θ). Right panel: stiffness (kj,elas) as function of angle(θ).

2.7 Co-contraction model

The net joint torque is the torque exerted by the agonist minus the torque exerted by the antagonist.

$$T_j = T_{ag} - T_{an} \tag{7}$$

with T_j the net joint torque, T_{ag} the torque exerted by the agonist and T_{an} the torque exerted by the antagonist. Joint SRS is the sum of the individual stiffness contributions of the agonist and antagonist muscles

$$k_{srs,m} = k_{srs,an} + k_{srs,at} \tag{8}$$

The relation between stiffness and torque is given by:

$$\begin{aligned} k_{srs,ag} &= \alpha_{ag} \cdot T_{ag} \\ k_{srs,an} &= \alpha_{an} \cdot T_{an} \end{aligned} \tag{9}$$

where α_{an} and α_{ag} are the gradients of the SRS-torque relation of the agonist and antagonist respectively, which makes the overall SRS-torque relation

$$T_j = \frac{k_{srs,ag}}{\alpha_{ag}} - \frac{k_{srs,an}}{\alpha_{an}} \tag{10}$$

and the joint SRS

$$k_{srs,j} = \alpha_{ag} \cdot T_{ag} + \alpha_{an} \cdot T_{an} \tag{11}$$

Fig. 6 shows the results of a simulation of (11) at different co-contraction levels, where $\alpha_{an}= \alpha_{ag}$=6/rad (van Eesbeek et al., 2010). Without co-contraction one muscle will contract while the antagonist remains relaxed (Fig. 6, red). The grey shaded area in Fig. 6 shows the whole range of physical potential of the joint at various co-contraction levels. In case the agonist and antagonists exert equal torques, SRS values lie on the

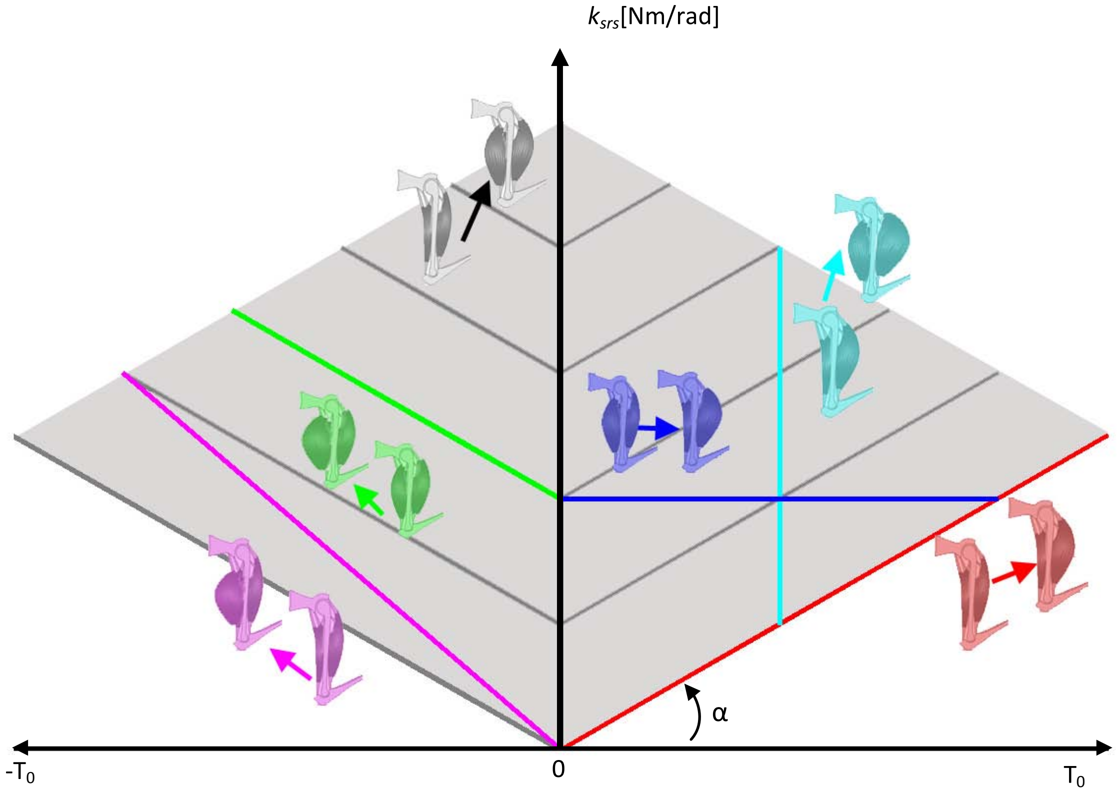

Fig. 6, Theoretical model of the SRS-torque relation at different levels of co-contraction the shaded area indicates the physical potential of the joint. $-T_0$ indicates a torque in flexion direction $+T_0$ indicates in extension direction of a joint. Increased volume of the muscle indicates an increased contraction level. Red: Muscle contraction without co-contraction. Magenta: Increased muscle stiffness in the higher contraction level caused by an increased level of type II fibers. Green: Increased contraction level in rest. Agonist muscle activation does not change while antognist activation increases. Black: Equal contraction level of agonist and antagonist. Cyan: agonist and antagonist activation increases equally. Blue: Activation of the agonist increases while activation of the antagonist decreases.

vertical (T_0=0 Nm) axis (Fig. 6, black). As mentioned before the SRS-torque relation can be altered in movement disorder or elderly muscles, which can result in the following altered SRS-torque relations. The first is caused by an increased contraction level in rest causing a high SRS value at 0Nm. When a torque is exerted the torque applied by the agonist is higher than the torque exerted by the antagonist, which would shift the SRS-torque relation upwards (Fig. 6, green). In this scenario α is similar as in healthy subjects. Another possible change is caused by the increase of type I muscle fibers. As mentioned before SRS is higher in type I compared to type II fibers. Type I fibers are always recruited before type II fibers. SRS of muscles containing a higher amount of type I fibers might increase faster at the higher torque or co-contraction levels (Fig. 6, magenta). Upon excitation of the agonist the antagonist is also activated, which requires an even greater activation of the agonist to exert a torque (Fig. 6, cyan), the value of α is increased in this case. When upon activation of the agonist the antagonist deactivates, SRS will be equal while torque increases (Fig 6, blue). In all cases the physical range is decreased, which makes it more difficult to measure α.

When α_{ag} and α_{an} are not altered and similar in magnitude, the contribution to of each individual muscle can be calculated with

$$T_{ag} = T_{net} + \frac{k_{srs,j} - \alpha \cdot T_{net}}{2\alpha} \tag{12}$$

$$T_{an} = \frac{k_{srs,j} - \alpha \cdot T_{net}}{2\alpha} \tag{13}$$

3 Results

Fig. 4 shows typical recordings of the lever torque and the motor angle in two directions. Fig. 5 shows a typical result of the measured and predicted torque on the handle.

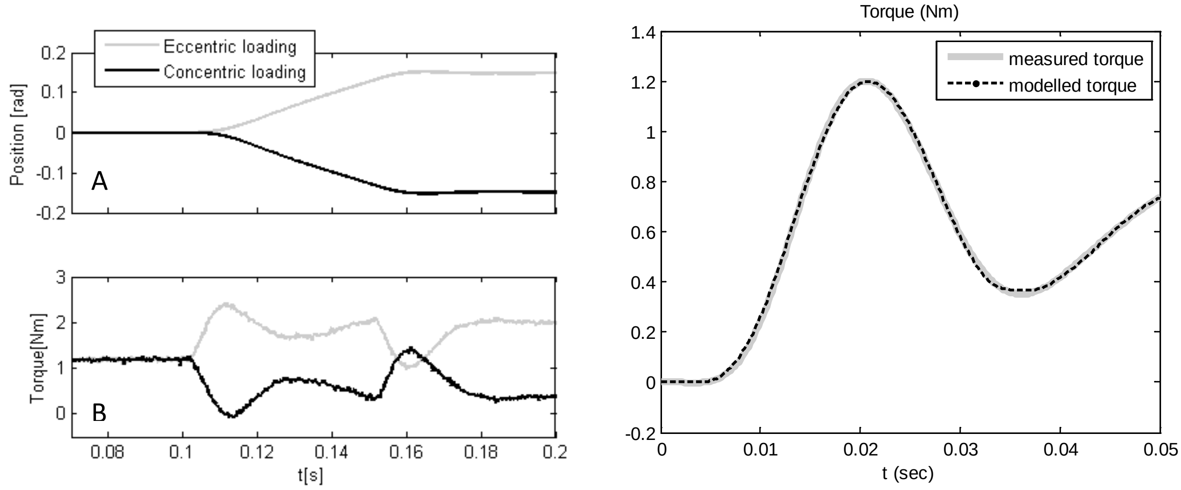

Fig. 7 Left panel: typical position and torque recordings of the handle for a subject ($T0$ = 1.2 Nm, 1.95 rad / s) at expanded time axes. A: measured angle. B: measured torque. Right panel: typical model prediction of the torque on the handle.

3.1 Time frame

In general it was more difficult to find a good fit for the task where subjects did not exert any torque (T_0=0Nm) (Fig.8, trial number 1-6). Best fits for both young and elderly groups were found for an observation window between 50 and 55 ms. On average, when T_0=0Nm was not taken into account SEM was best at 55 ms (SEM=0.022) and VAF was very good (more than 0.97) for windows below 60 ms. VAFs dicreased when the observation time was increased to above 60ms.

To summarize, best fits were found at a 50 ms observation window, which is supported by the high VAF values and low SEM values.

3.2 Stiffness curvature

Differences in results were found between the 0Nm condition and the conditions where subjects had to exert a torque on the handle. At the condition were subjects did not exert any torque (T_0=0Nm) a_s=10 and a_s=$10^{1.5}$ resulted in the best fits with VAF values more than 0.998 and SEM values of 0.0395 compared to SEM values of 0.239 at a_s=10^2 (Fig. 8). At the higher torque levels slightly better results were found for a_s>$10^{1.5}$ (Fig. 8). In elderly subjects similar results were found.

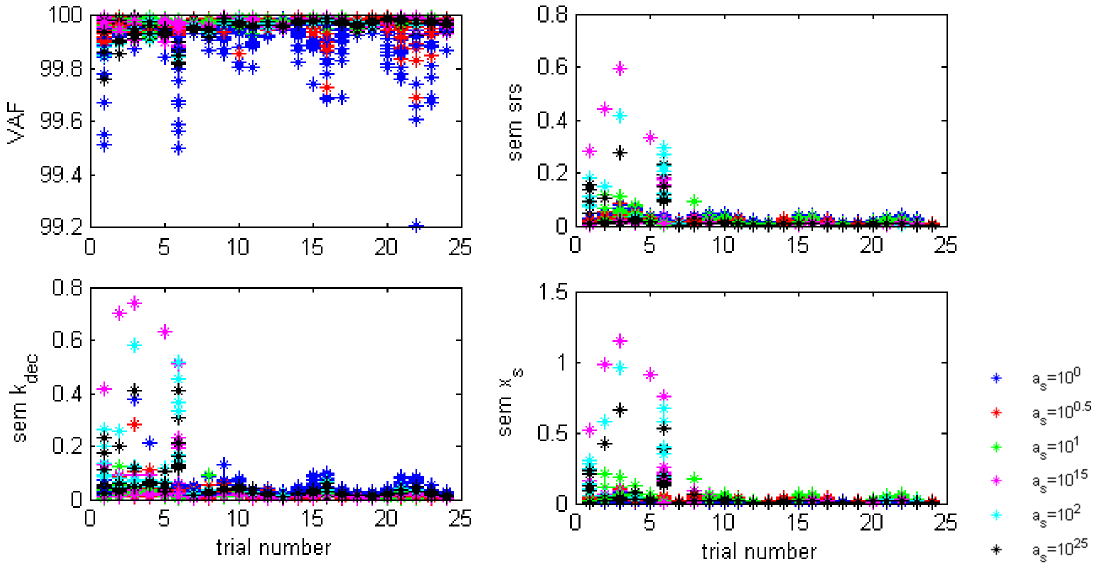

Torque level and movement velocity per trial number.

	-3.25m/s	-1.92m/s	-0.65ms	-0.65ms	1.92m/s	3.25m/s
0Nm	1	2	3	4	5	6
0.6Nm	7	8	9	10	11	12
1.2Nm	13	14	15	16	17	18
1.8Nm	19	20	21	22	23	24

Fig 8, VAF and sem values of the identified paramaters, srs, k_{dec} and x_s at different values of a_s for all trials and subjects. The table indicates the force and velocity levels per trial.

3.3 Eccentric and concentric loading

For all subjects in all conditions, the model was able to describe the recorded torque accurately with VAF values of 0.998 ± 0.0038 and mean SEM values of 0.0238. Fig. 9 shows all model parameters against torque for eccentric and concentric loading conditions, averaged over subjects and trials. The decrease in stiffness beyond SRS, k_{dec}, was higher for concentric loading ($p=0.048$, $F=5.42$). For all other model parameters, including SRS and EL, no significant differences were found between eccentric and concentric loading for all torque levels and velocities.

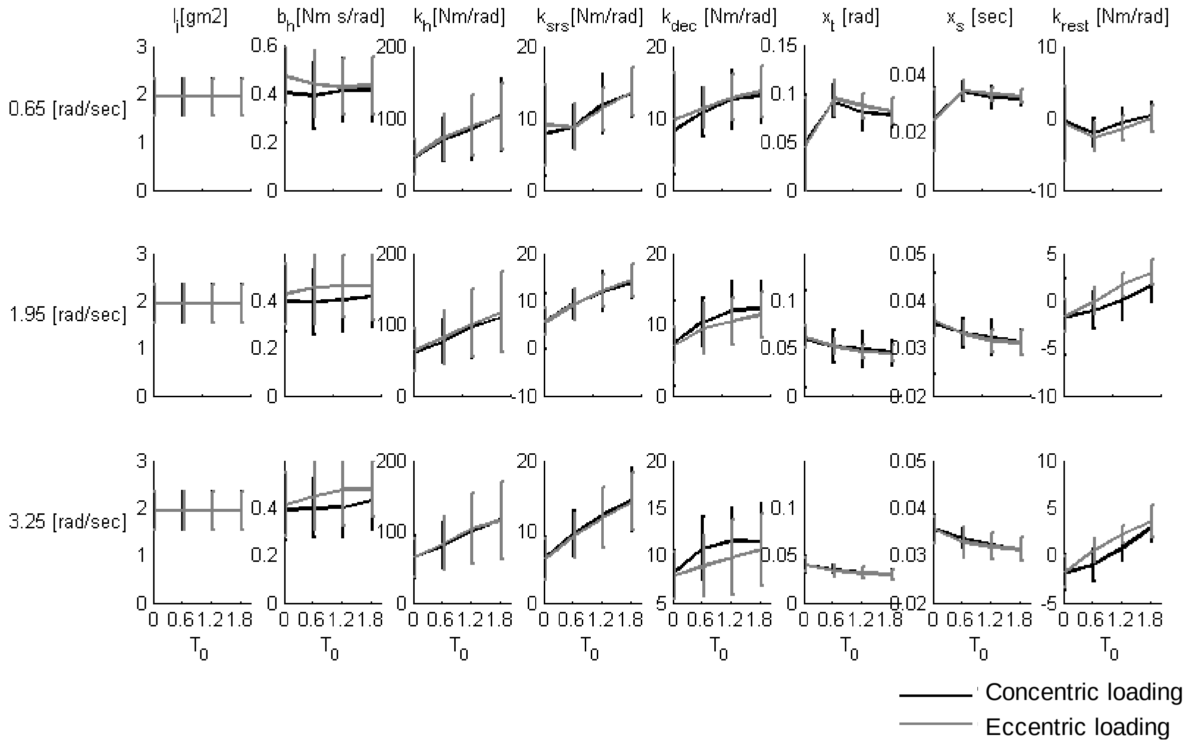

Fig. 9, Estimated model parameters averaged over all subjects and observations (mean ± 1 s. d.) for the three movement velocities (upper, middle and bottom row), eccentric and concentric direction (grey and black) and the four incremented torque levels (horizontal axes). The SRS period, x_t, was derived from the estimated parameters and the model simulation and taken as the elapsed time from the onset of the RaH to the time instance where the (simulated) joint angle was equal to the elastic limit. The stiffness beyond the elastic limit, k_{after} (bottom row), was taken equal to $k_{srs} – k_{dec}$.

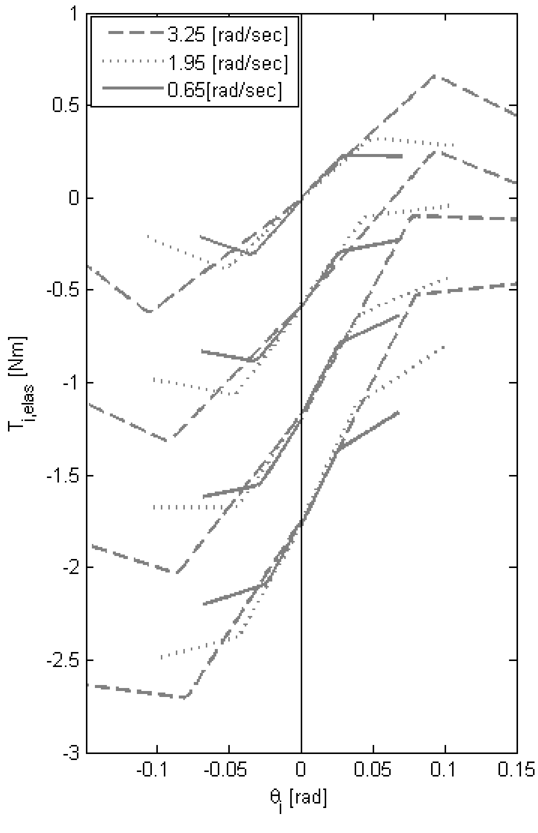

Fig. 10, Typical model predictions of the elastic muscle–tendon wrist torque and kdec. Elastic torque (Tj,elas) against muscle-tendon lengthening as described by the joint angle θj. for the three movement velocities. Concentric and eccentric loading is shown at –θ and + θ respectively.

3.4 Co contraction

Five out of six participants did not show any significant increase of SRS or k_{dec} with co-contraction level. All parameters were estimated accurately with VAF values of 0.998 and SEM values of 0.0179 for the values with co-contraction.

Torque-SRS

One subject showed an increase of SRS with co-contraction level ($p<0.001$, $F=139.96$) (Fig. 11A). In the same subject the decrease of stiffness beyond SRS, k_{dec} increased with co-contraction level ($p=0.011$, $F=15.87$) (Fig. 11B).

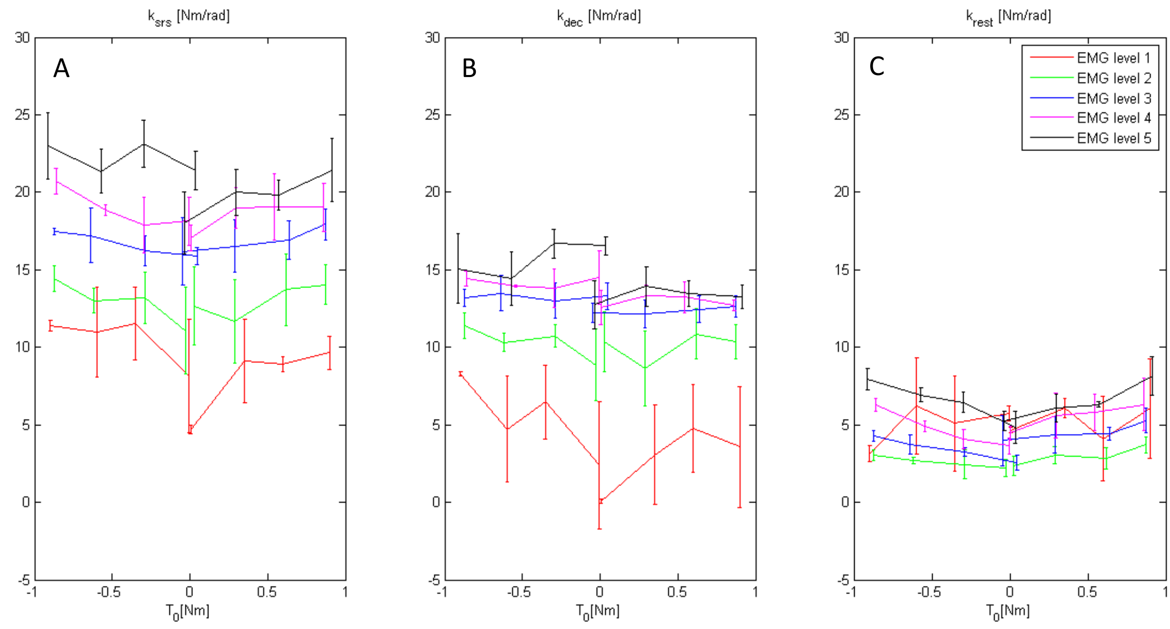

Fig. 11, Estimated model parameters for one subjects average over three observations (mean ± 1 s. d.) at a velocity of 3.25m/s for four incremented torque levels (horizontal axes) and vife co-contraction levels. A: k_{srs}, B: k_{dec}, C: k_{rest}

EMG-SRS

SRS should increase with muscle activity. A correlation between the EMG activity before SRS and SRS was identified by calculating the highest correlation coefficient. In all subjects an increase of SRS with the sum of the normalized EMG signals was found. A second order regression analysis showed an increase of SRS in every subject (Fig. 12, left panel) however a definite relation between SRS and summed EMG was not found. K_{dec} also increased with the EMG (Fig. 12, right panel) however the same indistinct relation as between SRS and EMG was found.

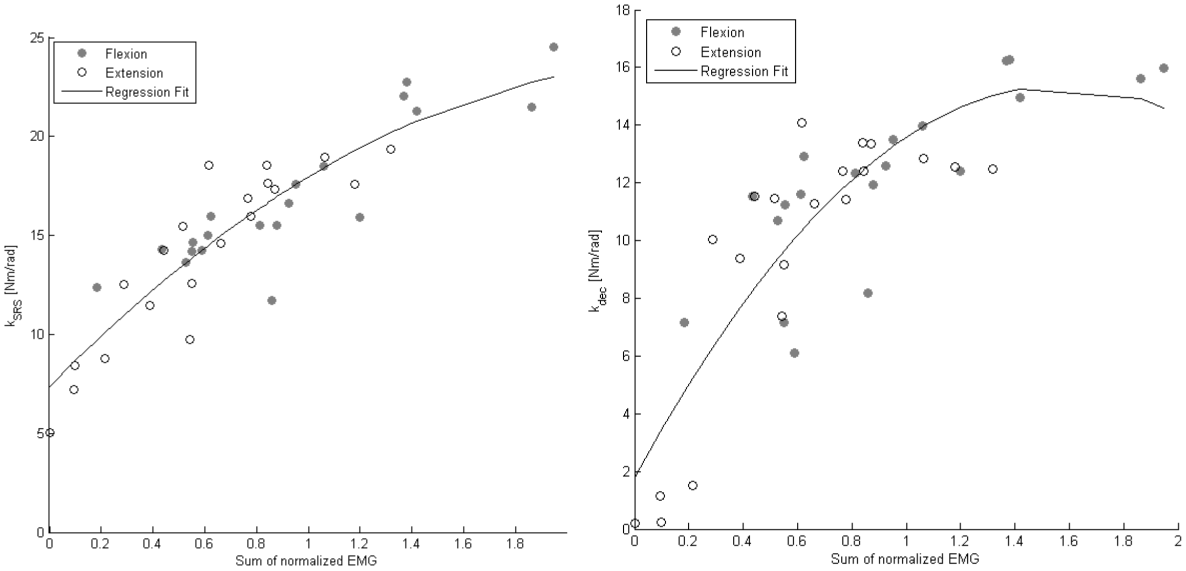

Fig. 12 Correlation between the summed and normalized EMG of the agonist and antagonist and SRS and k_{dec}, left panel: SRS as a function of summed EMG. Right panel: k_{dec} as a function of summed EMG

Torque agonist and antagonist

Individual torque contribution was calculated with (12), where α was taken to be 6/rad. Results showed an increase of SRS with both flexor and extensor torque (Fig. 13).

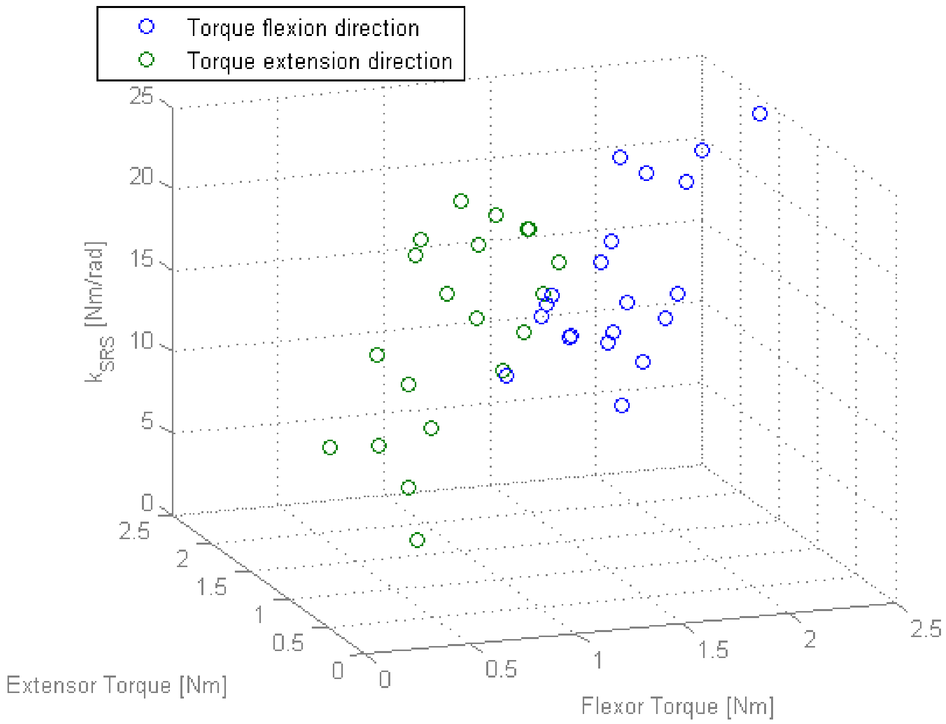

Fig. 13, Extensor and flexor torque contributions to co-contraction with respect to SRS.

3.5 Elderly

Fig.14 shows the results of SRS, the elastic limit (x_s) and k_{dec} against torque at highest velocity level for young and elderly subjects. No significant differences for all parameters in all conditions were found between young and elderly subjects. A small difference in

SRS between young and elderly subjects was observed in the 0Nm torque condition, which is however not proved to be significant.

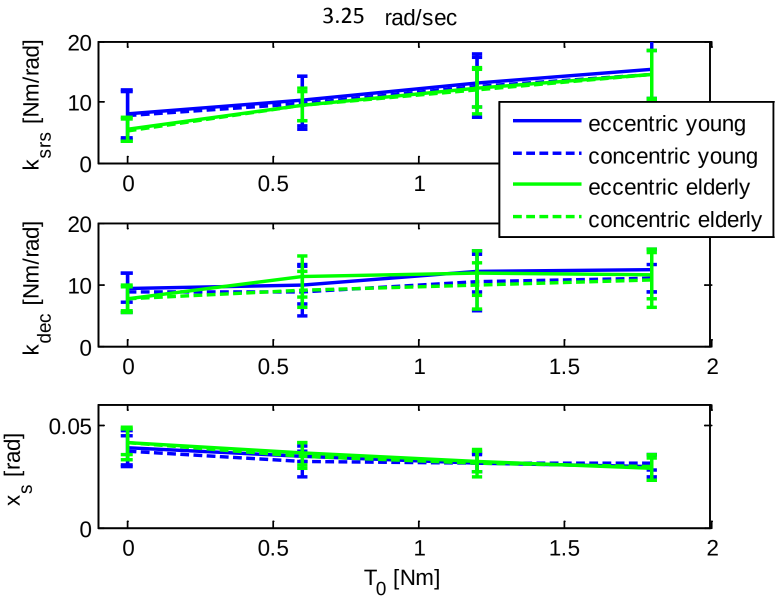

Fig. 14, Pooled parameter results. Parameter results with one time standard deviation for concentric and eccentric and elderly and young subjects at 3.25 rad/sec, averaged over observations and subjects

4 Discussion

The aim of this study was to examine the effect of eccentric and concentric loading and co-contraction on SRS, EL and the decrease in stiffness after SRS, k_{dec} in young and elderly subjects and to test the curvature of the transition between SRS and k_{rest} and the used time frame of the identification method. SRS, EL and the decrease in stiffness beyond SRS were estimated from in vivo recordings of wrist torque and angle. Results showed that SRS and EL in concentric loading did not differ from eccentric loading conditions. The decrease in stiffness beyond EL, k_{dec}, was increased in concentric condition. Results of the co-contraction measurements showed that SRS increased with co-contraction level, however not all subjects were able to control a co-contraction level with the use of EMG. Results on measurements on elderly showed that SRS, k_{dec} and EL did not differ significantly in elderly subjects compared to young subjects.

Time frame

Best fits were found at a 50ms time frame. VAFs were worse when the time frame was increased to >60ms, which was as expected due to the increased number of data points. Another possible cause of the decrease in VAF is caused by a drop in muscle activation after a time period of 60ms causing a decrease in stiffness, which is not described by the model. The task description for the subjects was not defined after the RAH movement. In addition the effect of reflexes could be more pronounced after 50ms, which is also not included in the model.

Curvature

Fits were found to be good for $a_s>10^{1.5}$ for tasks were subjects had to exert a torque to the handle. At the task where subjects did not had to exert a torque (T_0=0Nm), lower values of a_s resulted in better fits. Worse fits at T_0=0Nm which might be caused by less attached cross-bridges. A low SRS at T_0=0Nm task could result in a worse signal to noise ratio. In addition viscous behavior of the muscle could be more pronounced due to less stiffness contribution of the low amount of attached cross-bridges.

Concentric loading

Elastic behavior was examined during brief ramp and hold (RaH) movements applied in both flexion and extension direction. In both eccentric and concentric loading condition a good model fit was found for the biphasic stiffness patter, which makes it evident that SRS is also present in concentric loading. Corresponding results were found in experiments on fiber (Campbell and Lakie, 1998; Roots et al., 2007) as well as on muscle level (Herzog and Leonard, 1997; Joyce et al., 1969; Rack and Westbury, 1974), where force response during a ramp shortening or lengthening showed a steep slope at the start of a movement followed by a more gradual change in slope. Although this muscle behavior was not referred to SRS by the authors, it indicated a high stiffness at the start of a movement and less stiffness thereafter.
The decrease in stiffness beyond EL (k_{dec}) was found to be larger in concentric compared to eccentric loading. The difference between k_{dec} in eccentric and concentric condition seems to increase with velocity, which is however, not proved to be significant. The force velocity relation of (Hill, 1938) shows a exponential force decrease as the velocity of shortening increases. In contrast, when a muscle is actively lengthened, the force developed by the muscle increases with increasing speeds of lengthening. In a study by (Roots et al., 2007) on intact muscle fibers, Hills force velocity relation was reproduced by applying ramp shortening and lengthening movements at different velocities. The tension at the second part of the length tension response was plotted against the velocity of shortening or lengthening providing the same relation as in Hill. The force velocity relation is also visualized in Fig. 10, where the slope of the second part of the torque-angle relation increases with lengthening velocity and reversely changes with shortening velocity.

Elderly

Although changes in aging muscles such as a loss of type I muscle fibers, an increased level of fat and connective tissue, altered moment arms and fiber pennation angle can alter cross-bridge dynamics, no significant differences were found here between young and elderly subjects.

To generate a muscle force a certain number of cross bridges need to be connected; in this case, when a torque is exerted SRS would be similar in elderly compared to young subjects. However in aging muscles relatively more type I fibers are present and studies on skinned fibers and single motor units have indicated that type I fibers are stiffer than type II fibers in the SRS range (Malamud et al., 1996), which could make SRS increase faster upon activation in elderly. This increase would me more pronounced at higher contraction levels were normally more type II fibers are activated. Differences might be found at contraction levels higher than used in this study. Cui et al. (2007) showed that motor unit composition has little effect on the short-range stiffness, which might be why no differences between young and elderly subject was found.

With aging changes in muscle tissue gets more severe. In the group used for this changes might not jet been severe enough to be notable. Another reason why no differences were found could be the canceling effect of the many changes in the aging muscle.

A small difference is found in the 0Nm torque condition, which is however not proved to be significant. In the 'relax' task where subjects did not exert any torque a small amount of SRS was identified, indicating low levels of attached cross bridges. In elderly the cross sectional area of the muscle is decreased (Morse et al., 2005), which could be the cause of lower SRS at the T_0=0Nm task. An increase in the number of subjects could indicate wetter the assumed difference in the 0Nm condition is significant.

Co-contraction

One subject showed as expected an increase of SRS and k_{dec} with co-contraction level. Five out of six participants did however not show any significant increase of SRS or k_{dec} with co-contraction level as defined in the experiment. The performance of the subjects during the experiment can cause variation in the results, which can probably be explained by the difficulty of keeping an EMG signal on one level for a period of 0.5s, causing an indefinite relation between the requested co-contraction level and EMG level. The relation between EMG and SRS showed however that a relation between summed EMG of the agonist and antagonist and actual co-contraction level exists. It is questionable wetter EMG is the right measure for muscle activity. EMG has its limitations. EMG is a relative measure due to the dependency of the amplitude of the EMG signal on the distance between muscle and recording electrodes and the localization of the electrodes relative to the anatomical structures of the muscle. EMG levels between subjects are not comparable. Patients with an increased muscle tone have no definite relation between EMG and the corresponding muscle force.

In stroke survivors unknown combinations of altered passive tissue characteristics, active cross-bridge dynamics and reflexive feedback results in altered joint stiffness (Burne et al., 2005; Meskers et al., 2009; Mirbagheri et al., 2001). The resulting movement disorders expose through reduced or altered muscle force and muscle force distribution around the joints, the so called load sharing. Current clinical tests at joint level cannot discriminate between the active and the passive (connective) tissue properties. SRS is shown to identify the contribution of the active muscle components to joint stiffness. It is also shown the contribution of individual torque contribution of the agonist and antagonist can be estimated, which provides an alternative besides EMG to quantify co-contraction. This technique is expected to be important for clinical purpose especially in movement disorders where the active muscle components are affected.

5 Conclusion

SRS is equal in concentric and eccentric loading which shows that cross-bridge behavior is elastic in both directions for small movements. The decrease of stiffness after SRS, k_{dec} is greater in concentric loading compared to eccentric loading, indicating the decrease in attached cross bridges during shortening. The results corresponded well to the muscle force velocity relation.

Alternated joint dynamics are present in elderly however this did not result in an altered joint SRS in the measured conditions. It could be concluded that muscles did not change significantly on the age of 62 or that the changes on muscle and joint level in the aging joint can cancel each other. Differences might be found at highest or lowest contraction levels caused by relatively more type I or smaller muscle in the elderly respectively.

Increased muscle activity of both agonist and antagonist muscle results in a higher level of short range stiffness and a greater decrease of stiffness after SRS, k_{dec}. Only one measurement resulted in a good estimation of the SRS-co-contraction relation. EMG appears to cause indefinite relations between co-contraction and SRS. Individual torque contributions per muscle group were calculated, which gives a rate of co-contraction by only measuring wrist torque and identifying SRS, without the use of EMG. By means of SRS we will be able to quantify the contribution of the wrist flexors and extensors cross-bridge dynamics relative to joint torque and joint stiffness. This technique can be used for clinical applications in many muscular diseases where joint torque-stiffness relation is altered.

Reference List

Burne JA, Carleton VL, O'Dwyer NJ. 2005. The spasticity paradox: movement disorder or disorder of resting limbs? Journal of Neurology Neurosurgery and Psychiatry 76:47-54.
Campbell KS, Lakie M. 1998. A cross-bridge mechanism can explain the thixotropic short-range elastic component of relaxed frog skeletal muscle. Journal of Physiology-London 510:941-962.
Campbell KS, Moss RL. 2002. History-dependent mechanical properties of permeabilized rat soleus muscle fibers. Biophysical Journal 82:929-943.
Campbell KS, Patel JR, Moss RL. 2003. Cycling cross-bridges increase myocardial stiffness at submaximal levels of Ca2+ activation. Biophysical Journal 84:3807-3815.
Cui L, Perreault EJ, Sandercock TG. 2007. Motor unit composition has little effect on the short-range stiffness of feline medial gastrocnemius muscle. Journal of Applied Physiology 103:796-802.
de Vlugt E, van Eesbeek S, Baines P, Hilte J, Meskers CGM, de Groot JH. Short Range Stiffness Elastic Limit Depends on Joint Velocity. In. submitted.
Herzog W, Leonard TR. 1997. Depression of cat soleus forces following isokinetic shortening. Journal of Biomechanics 30:865-872.
Hill AV. 1938. The heat of shortening and the dynamic constants of muscle. Proceedings of the Royal Society of London Series B-Biological Sciences 126:136-195.
Joyce GC, Rack PMH, Westbury DR. 1969. Mechanical Properties of Cat Soleus Muscle During Controlled Lengthening and Shortening Movements. Journal of Physiology-London 204:461-&.
Malamud JG, Godt RE, Nichols TR. 1996. Relationship between short-range stiffness and yielding in type-identified, chemically skinned muscle fibers from the cat triceps surae muscles. Journal of Neurophysiology 76:2280-2289.
Meskers CGM, Schouten AC, de Groot JH, de Vlugt E, van Hilten BJJ, Van der Helm FCT, Arendzen HJH. 2009. Muscle weakness and lack of reflex gain adaptation predominate during post-stroke posture control of the wrist. Journal of Neuroengineering and Rehabilitation 6.
Mirbagheri MM, Barbeau H, Ladouceur M, Kearney RE. 2001. Intrinsic and reflex stiffness in normal and spastic, spinal cord injured subjects. Experimental Brain Research 141:446-459.
Morse CI, Thom JM, Reeves ND, Birch KM, Narici MV. 2005. In vivo physiological cross-sectional area and specific force are reduced in the gastrocnemius of elderly men. Journal of Applied Physiology 99:1050-1055.
Petit J, Filippi GM, Emonetdenand F, Hunt CC, Laporte Y. 1990. Changes in Muscle-Stiffness Produced by Motor Units of Different Types in Peroneus Longus Muscle of Cat. Journal of Neurophysiology 63:190-197.
Rack PM, Westbury DR. 1974. The short range stiffness of active mammalian muscle and its effect on mechanical properties. J. Physiol 240:331-350.
Ramamurthy B, Jones AD, Larsson L. 2003. Glutathione reverses early effects of glycation on myosin function. American Journal of Physiology-Cell Physiology 285:C419-C424.
Roots H, Offer GW, Ranatunga KW. 2007. Comparison of the tension responses to ramp shortening and lengthening in intact mammalian muscle fibres: crossbridge and non-crossbridge contributions. Journal of Muscle Research and Cell Motility 28:123-139.
Schouten AC, de Vlugt E, van Hilten JJB, van der Helm FCT. 2006. Design of a torque-controlled manipulator to analyse the admittance of the wrist joint. Journal of Neuroscience Methods 154:134-141.
van Eesbeek S, de Groot JH, van der Helm FC, de Vlugt E. 2010. In vivo estimation of the short-range stiffness of cross-bridges from joint rotation. J. Biomech. 43:2539-2547.
Vandervoort AA. 2002. Aging of the human neuromuscular system. Muscle & Nerve 25:17-25.
Walmsley B, Proske U. 1981. Comparison of stiffness of soleus and medial gastrocnemius muscles in cats. J. Neurophysiol. 46:250-259.